

Reinforcement Learning with Data Bootstrapping for Dynamic Subgoal Pursuit in Humanoid Robot Navigation

Chengyang Peng¹, Zhihao Zhang², Shiting Gong³, Sankalp Agrawal², Keith A. Redmill², and Ayonga Hereid¹

Abstract—Safe and real-time navigation is fundamental for humanoid robot applications. However, existing bipedal robot navigation frameworks often struggle to balance computational efficiency with the precision required for stable locomotion. We propose a novel hierarchical framework that continuously generates dynamic subgoals to guide the robot through cluttered environments. Our method comprises a high-level reinforcement learning (RL) planner for subgoal selection in a robot-centric coordinate system and a low-level Model Predictive Control (MPC) based planner which produces robust walking gaits to reach these subgoals. To expedite and stabilize the training process, we incorporate a data bootstrapping technique that leverages a model-based navigation approach to generate a diverse, informative dataset. We validate our method in simulation using the Agility Robotics Digit humanoid across multiple scenarios with random obstacles. Results show that our framework significantly improves navigation success rates and adaptability compared to both the original model-based method and other learning-based methods.

I. INTRODUCTION

Humanoid robots are increasingly demonstrating their adaptability to complex and crowded environments. Equipped with dexterous manipulation and versatile locomotion capabilities, these robots can navigate human environments and handle objects with precision, making them well-suited for tasks in logistics, public services, and entertainment. Because these tasks frequently take place in crowded environments, robust navigation capabilities are essential to ensure safe, efficient, and reliable performance. However, navigating these dynamic and often unpredictable settings poses significant challenges for bipedal robots given their underactuated and high-dimensional dynamics [1]–[3]. Current navigation frameworks commonly separate geometric path planning from real-time locomotion control, making it difficult to accommodate the nonlinear dynamics of bipedal robots and limiting their performance in unpredictable or crowded environment [4]–[7]. Moreover, discrepancies between the planned path and the executed trajectory are inevitable due to model inaccuracies, external disturbances, and dynamic constraints. Such deviations are especially critical for underactuated bipedal robots, where even minor errors can lead to instability or falls,

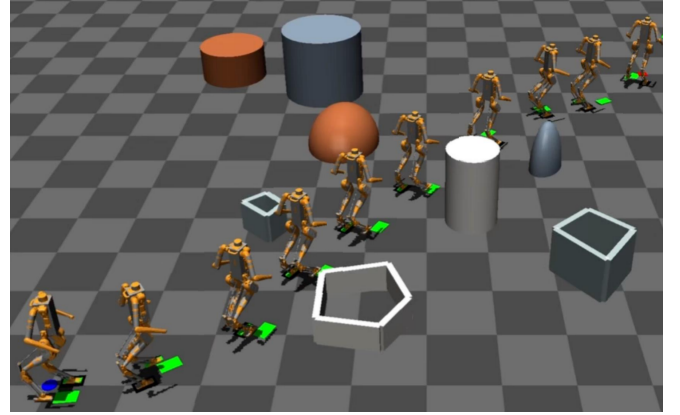


Fig. 1. A humanoid robot navigates around cluttered environment using our proposed sub-goal orientated framework.

underscoring the need for robust navigation methods [8]–[10].

Model-based methods are commonly used in bipedal locomotion control, formulating and solving constrained optimization problems to integrate path planning with robot dynamics. Many studies have developed trajectory optimization controllers based on whole-body dynamics [11]–[13] or reduced-order dynamics [14]–[17], leading to significant improvements in motion performance. In practice, these frameworks rely on simplified center-of-mass or foot-placement models, using Model Predictive Control (MPC) or Quadratic Programming (QP) to compute stable walking gaits. However, effectively integrating high-dimensional environmental information (e.g., occupancy maps) into these optimization problems is challenging, as it greatly increases the state space and number of constraints—ultimately slowing real-time computation. Moreover, the nonlinear coupling of the heading angle, turning rate, and other system states further complicates the optimization process [10], [18], [19]. While our previous work [20] attempted to mitigate these nonlinearities by precomputing heading angles, it still relies on a geometric approach and thus cannot fully leverage the flexibility of bipedal locomotion in cluttered environments.

Recent advances in learning-based methods have showcased their potential in handling nonlinearities and optimizing high-dimensional control problems, opening new avenues for addressing complex robot navigation challenges. Imitation learning, for instance, leverages deep neural networks to train policies that mimic expert behavior [21]–[23]. However, this approach relies heavily on high-quality expert data and lacks active environmental interaction, limiting its ability to

*This work was supported in part by the National Science Foundation under grant FRR-21441568.

¹Mechanical and Aerospace Engineering, The Ohio State University, Columbus, OH, USA. (peng.947, hereid.1)@osu.edu.

²Electrical and Computer Engineering, The Ohio State University, Columbus, OH, USA. (zhang.11606, agrawal.268, redmill.1)@osu.edu.

³Computer Science and Engineering, The Ohio State University, Columbus, OH, USA. (gong.663)@osu.edu.

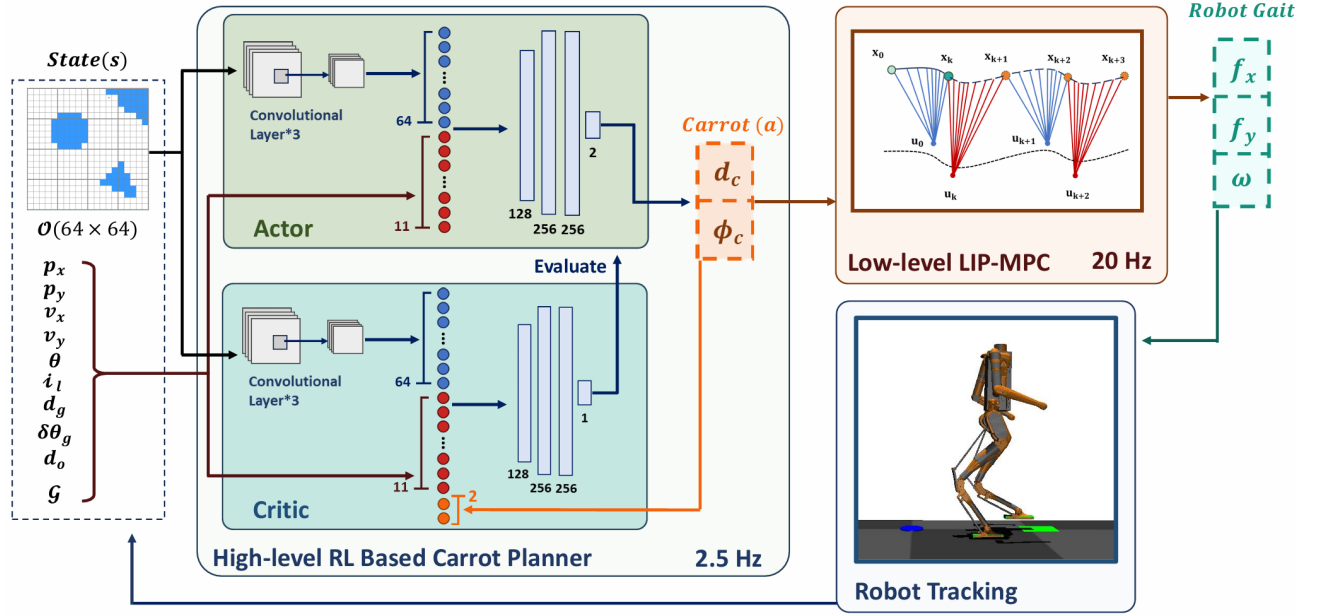


Fig. 2. Overall structure of the proposed hierarchical framework for humanoid navigation. The high-level RL-based planner uses local map data to continuously generate feasible dynamic subgoals that guide the robot step-by-step toward the global target, while the low-level MPC-based controller computes dynamically stable walking gaits that satisfy both motion and obstacle constraints to follow these subgoals.

generalize to novel scenarios. Reinforcement learning (RL) offers an alternative by enabling robots to learn navigation strategies through trial and error. RL-based approaches have shown promise in adaptive decision-making and motion planning [24]–[28]. Despite these advances, most existing RL navigation frameworks are tailored for wheeled robots with simpler kinematics and more straightforward action spaces. Moreover, RL methods are often hindered by sample inefficiency, as training from scratch without leveraging prior knowledge of the environment and robotic dynamics is challenging [29], [30]. This issue becomes even more pronounced in continuous action spaces and complex environments, where sparse or delayed reward signals increase the likelihood of converging to suboptimal solutions.

To bridge the gap between RL-based navigation and bipedal robot locomotion, we propose a novel hierarchical RL+model-based framework that divides the navigation task into two levels. At the high level, an RL planner dynamically generates subgoals in a local, robot-centric coordinate frame. At the low level, a gait planner based on a linear MPC leverages reduced-order bipedal dynamics to maintain dynamic stability and produce robust walking gaits for following these subgoals. By combining the adaptability of RL, capable of handling complex environments and unforeseen disturbances, with MPC’s predictive control of future states, our framework helps mitigate the risk of instability or falls in challenging scenarios. Furthermore, we adopt a demonstration data bootstrapping strategy, consistent with recent approaches in the literature [31]. Specifically, our replay buffer is populated with both online experiences and samples from an offline demonstration dataset generated by a model-based navigation method, which accelerates learning and enhances the

robustness of the learned navigation policies.

The rest of the paper is organized as follows: Section II details our Subgoal-Pursuit hierarchical framework. Section III introduces the training setup and procedure of the framework. Section IV evaluates its performance in simulation, comparing it with model-based frameworks and various state-of-the-art learning-based high-level planners. Finally, Section V concludes the contributions, limitations, and future work.

II. HIERARCHICAL BIPEDAL NAVIGATION FRAMEWORK

This section introduces a two-level hierarchical architecture for robust bipedal navigation and obstacle avoidance, as illustrated in Fig. 2. The central idea is to learn dynamic subgoals using only local map data and other state information, enabling the robot to navigate complex environments.

A. Reinforcement Learning for Dynamic Subgoal Planner

We formulate the problem of learning dynamic subgoals for bipedal navigation as a Markov Decision Process (MDP) defined by the tuple:

$$\mathcal{M} = (\mathcal{S}, \mathcal{A}, \mathcal{P}, r, \gamma), \quad (1)$$

where \mathcal{S} is the state space; \mathcal{A} is the action space; \mathcal{P} denotes the state transition model; $r : \mathcal{S} \times \mathcal{A} \rightarrow \mathbb{R}$ is a reward function and $\gamma \in (0, 1]$ is a discount factor.

State Space. To generate effective dynamic subgoals for navigation, the high-level RL planner must capture both environmental perception and the robot’s dynamic state. In this work, we assume that the robot’s perception is limited to a relatively small local region. To facilitate this, we construct a 64×64 local occupancy grid map centered on the robot, which spans a forward detection range of 4.5 m, a

backward detection range of 1.5 m, and a lateral width of 6 m. This occupancy map, denoted as \mathcal{O} , provides structured local perception data that enables the RL agent to accurately detect obstacles and plan safe maneuvers. In addition to the environmental data, the robot's locomotion state is a key feedback component of the state representation. Since the high-level planner generates a new subgoal at the beginning of each walking step, we represent the robot's reduced-dimensional step-to-step dynamics by capturing its center-of-mass (CoM) state at the start of each step. Moreover, to steer the robot toward a designated goal, we incorporate goal-related information—specifically, the goal position and the corresponding Euclidean distance and relative heading to the goal—into the state. Thus, the final state $s \in \mathcal{S}$ is defined as follows:

$$s = \{\mathcal{O}, p_x, p_y, v_x, v_y, \theta, i_l, d_g, \delta\theta_g, d_o, \mathcal{G}\}, \quad (2)$$

where \mathcal{O} denotes the occupancy map, $[p_x, p_y, v_x, v_y, \theta]$ represent the robot's CoM position, velocity, and heading angle in the world frame. i_l indicates the stance foot, with -1 for the left foot and 1 for the right foot. $[d_g, \delta\theta_g]$ denote the robot's Euclidean distance and relative heading to the goal, while d_o measures the distance to the nearest obstacle in the local map. Finally, \mathcal{G} represents the goal position in the world frame.

Action Space. The high-level planner defines its action $a \in \mathcal{A}$ as a dynamic subgoal specified in a robot-centric polar coordinate system. The action is represented as:

$$a = (d_c, \phi_c), \quad (3)$$

where d_c denotes the distance from the robot to the subgoal and ϕ_c indicates the direction relative to the robot's current heading. These parameters are constrained by the robot's physical capabilities, such as step length and turning limits, to ensure compatibility with the low-level MPC controller. In our implementation, d_c is limited to $[0, 3]$ meters, and ϕ_c is limited to $[-\pi/4, \pi/4]$ radians.

To model the stochastic policy $\pi(a|s)$ in the continuous action space, we use the Soft Actor-Critic (SAC) [32] algorithm. Specifically, the policy π is modeled as a Gaussian distribution, where actions are sampled as:

$$a \sim \pi(a|s) = \mathcal{N}(\mu_\pi(s), \sigma_\pi(s)). \quad (4)$$

Here, $\mu_\pi(s)$ and $\sigma_\pi(s)$ are the mean and standard deviation of the action distribution, which are the output of the policy network. The optimal policy is obtained by maximizing the expected cumulative discounted reward, expressed as:

$$\pi^* = \arg \max_{\pi} \mathbb{E}_{\pi} \left[\sum_t \gamma^t r(s[t], a[t]) + \alpha H(\pi(\cdot|s[t])) \right],$$

where $H(\pi(\cdot|s_t))$ represents the entropy term of the policy and α is the regularization factor. The policy maintains a balance between long-term optimality and sufficient exploration by leveraging SAC's entropy-regularized objective, ensuring robust navigation performance.

Network Structure. Since we use the SAC algorithm, our framework utilizes two neural networks: an actor network and a critic network. The actor network takes as input the heterogeneous state representation defined in (2) and generates dynamic subgoals—i.e., actions—according to (4). To process the heterogeneous data, the actor network is composed of two modules. First, a Convolutional Neural Network (CNN) processes the occupancy map. This CNN has three convolutional layers with 3×3 kernels, each followed by ReLU activation and max pooling to extract spatial features. The output of the final convolutional layer is flattened and passed through two fully connected layers, reducing the feature dimension to 64. Next, these 64-dimensional map features are concatenated with the remaining state information and are processed by four fully connected layers which output the parameters of a Gaussian distribution over the dynamic subgoals (actions). The critic network adopts a similar architecture, with the only difference being that its final output is a single scalar value representing the state-action value. The structure of the proposed actor-critic network is illustrated in Fig. 2.

Reward Function. Designing an effective reward function is crucial for reinforcement learning-based navigation, as it directly influences the generation of feasible dynamic subgoals that guide the robot toward the goal while ensuring obstacle avoidance and smooth locomotion. To achieve this, we define the total reward function as a weighted sum of several sub-rewards:

$$r = \mathbf{w}[r_g, r_\theta, r_a, r_v, r_o]^T + R_F, \quad (5)$$

where r_g, r_θ, r_a, r_v and r_o are sub-reward functions that address key aspects of bipedal navigation. Each reward term is normalized within $[0, 1]$ to maintain numerical stability during training. In this work, we choose the weight vector as $\mathbf{w} = [0.2, 0.1, 0.25, 0.2, 0.25]$ to ensure a balanced learning process. R_F is the terminal reward (and penalty) computed at the end of a navigation episode.

Goal Proximity Reward. To encourage goal-directed movement, we introduce a goal proximity reward r_g that measures the reduction in distance $\Delta d_g = d_g[t-1] - d_g[t]$ to the goal between consecutive time steps. This reward is defined as:

$$r_g[t] = \begin{cases} b_g + a_g \Delta d_g[t] & \text{if } \Delta d_g[t] \geq 0 \\ 0 & \text{otherwise} \end{cases}, \quad (6)$$

where b_g is a baseline reward granted when the distance to the goal does not increase and a_g is a scaling factor that encourages a greater reduction in the goal distance.

Heading Alignment Reward. To promote proper alignment of the robot's orientation with the goal direction, we introduce a heading alignment reward r_θ . We use a cubic function to penalize large heading errors:

$$r_\theta[t] = \begin{cases} 1 - a_\theta \|\delta\theta_g[t]\|^3 & \text{if } \|\delta\theta_g[t]\| \leq \pi/6 \\ 0 & \text{otherwise} \end{cases}, \quad (7)$$

where a_θ is a scaling factor that penalizes deviations from the goal direction.

Action Smoothness Reward.: To promote smooth motion, we define an action smoothness reward r_a that encourages consistent turning and gradual velocity changes. This reward consists of two components: one that incentivizes forward motion and another that penalizes abrupt action variations. The reward is formulated as:

$$r_a[t] = q_a r_p[t] + (1 - q_a) r_s[t], \quad (8)$$

where $r_p := \|d_c\|_d - \|\phi_c\|_\phi$ encourages the robot to make progress toward the goal while minimizing unnecessary turns, whereas $r_s[t] := 1 - (a[t] - a[t-1])$ penalizes large deviations between consecutive actions to ensure smooth transitions, and $q_a \in [0, 1]$ is a scaling factor that balances the weight for each component. Since the distance d_c and heading ϕ_c are defined on different scales, we use the separate normalization functions, $\|\cdot\|_d$ for distance and $\|\cdot\|_\phi$ for heading, to bring them to a same scale.

Velocity Reward.: Since bipedal locomotion involves both longitudinal (v_x) and lateral (v_y) velocity components, we introduce a velocity reward r_v that encourages maintaining longitudinal velocity and discourages lateral movement. This reward is formulated as follows:

$$r_v[t] = q_v r_{v_x}[t] + (1 - q_v) r_{v_y}[t], \quad (9)$$

where q_v is a weighting factor that balances the contributions of the two velocity components, and

$$r_{v_x}[t] = \frac{1}{1 + e^{-a_v(v_x[t] - b_v)}}, \quad (10)$$

$$r_{v_y}[t] = \begin{cases} 1 & \text{if } \|v_y[t]\| \leq 0.4 \\ 0 & \text{otherwise} \end{cases}, \quad (11)$$

where a_v is a scaling factor that encourages faster forward velocities and b_v is a baseline (recommended) forward velocity. This formulation ensures that the robot is incentivized to maintain a desired forward velocity while minimizing undesirable lateral movements.

Collision Avoidance Reward.: To enhance safety, we incorporate a collision avoidance reward r_o , inspired by our previous work with control barrier functions [20]. This reward is formulated using the half-plane distance to the closest obstacle:

$$r_o[t] = h(p_x[t], p_y[t]) + (\zeta - 1)h(p_x[t-1], p_y[t-1]), \quad (12)$$

where $h(p_x[t], p_y[t])$ is the linear function that measures the distance to the half-plane of the closest obstacles at time t , and $\zeta \in (0, 1]$ is a scaling parameter of the barrier condition. This formulation rewards the robot for increasing its distance from obstacles over consecutive time steps, thereby promoting safer navigation.

Terminal Reward and Penalty. In bipedal robot navigation, several terminal conditions can occur, including reaching the goal, colliding with obstacles, falling, and time-out. To account for these scenarios, we design specific rewards and

penalties as follows:

$$R_F = \begin{cases} 60e^{-\frac{0.4 \cdot N_{step}}{T_{max}}} + 40 & \text{Goal Reached} \\ -80 & \text{Failure} \\ -70 & \text{Time-out} \end{cases}, \quad (13)$$

where N_{step} stands for the number of steps taken before reaching the goal and T_{max} is the maximum time length for each training episode. The goal-reaching reward incorporates an exponential decay based on the number of steps to encourage faster navigation, while a large penalty is assigned to failure cases, such as colliding and falling. A slightly lower penalty is assigned to time-out scenarios, as it suggests the agent continues to explore rather than failing abruptly.

B. LIP based linear MPC for Stable Gait Planning

The low-level MPC-based gait controller receives a sub-goal generated by the high-level RL planner at the beginning of each step and generates a sequence of walking gaits based on the reduced dimensional Linear Inverted Pendulum (LIP) model [10], [14], [20].

Under the assumption that the robot's CoM height and centroidal momentum remain constant, the CoM dynamics in the x-y plane of a bipedal robot can be approximated using a simple linear inverted pendulum (LIP) model [14]. When the stance ankle is passive, akin to a point contact, the continuous dynamics within a walking step become autonomous, meaning that the progression of the robot's CoM states depends solely on its state at the beginning of the step. At impact, the CoM position (p_x, p_y) is reset relative to the new stance foot, thereby updating the initial conditions for the subsequent step. Consequently, our MPC planner formulates an optimal control problem for gait planning based on these step-to-step discrete dynamics, using the swing foot stepping positions (f_x, f_y) as control inputs. Additionally, as introduced in our previous work [20], the heading angle ϕ is incorporated into the state as a single integrator of the turning rate ω . Let $\mathbf{x} := [p_x, v_x, p_y, v_y, \theta]^T \in \mathcal{X} \subset \mathbb{R}^5$ denote the state vector and $\mathbf{u} := [f_x, f_y, \omega]^T \in \mathcal{U} \subset \mathbb{R}^3$ represent the control inputs. Assuming a constant step duration T , the step-to-step LIP dynamics with heading angle can be expressed as a discrete time linear control system:

$$\mathbf{x}_{k+1} = \mathbf{A}_L \mathbf{x}_k + \mathbf{B}_L \mathbf{u}_k. \quad (14)$$

To determine optimal stepping positions and turning rates that enables the robot to follow dynamic subgoals, we formulate an LIP-based Model Predictive Control (LIP-MPC) as the low-level planner. We define a quadratic cost function based on the Euclidean distance between the robot's CoM position at the beginning of every step and the subgoal (c_x, c_y) as follows:

$$q(\mathbf{x}_k) = (p_{x_k} - c_x)^2 + (p_{y_k} - c_y)^2 \quad \forall k \in [1, N], \quad (15)$$

with N being the number of prediction steps. In addition, our formulation incorporates several kinematic and path constraints—including those on velocity, reachability, and maneuverability—to ensure feasible and safe motions. For

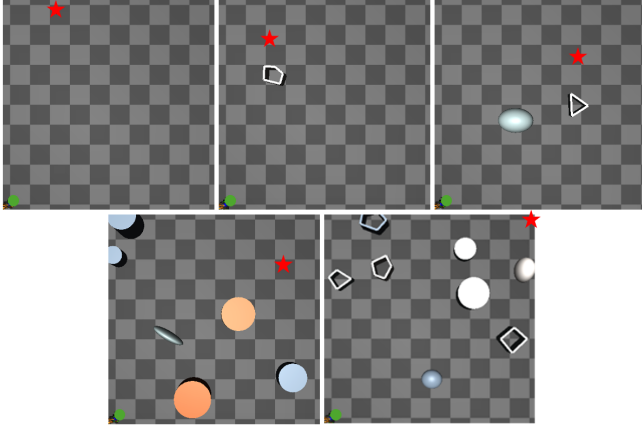


Fig. 3. Five representative environments from the 50 randomly generated training environments. Here, green dots represent initial positions, and red stars represent goal positions.

further details on the construction of these constraints and the overall MPC formulation, please refer to our previous work in [20]. In this work, we set the robot’s desired height to $H = 1$, the step duration to $T = 0.4$ s, and a prediction horizon to $N = 3$.

Since these constraints are evaluated in the local coordinate frame, they are inherently nonlinear. To linearize them, we map the direction to the subgoal ϕ_c to the turning rate control ω_k at each prediction step in the MPC using the relationship:

$$\omega_k = \frac{\phi_c}{NT}. \quad (16)$$

Benefiting from the high-level RL planner generating dynamic subgoals at each step, the resulting optimization problem in the low-level MPC reduces to a Linear Constraints Quadratic Problem (LCQP). This approach enables the MPC to stabilize the walking process effectively by updating the stepping positions at a frequency of 20 Hz or faster.

III. POLICY LEARNING WITH DATA BOOTSTRAPPING

This section describes our reinforcement learning setup and procedure for developing a dynamic subgoal policy in humanoid navigation. To enhance learning efficiency, we employ a data bootstrapping approach that leverages offline expert demonstrations to initialize the learning process.

Training Setup. We use the Agility Robotics humanoid Digit as our testing platform in a MuJoCo simulation. For training the high-level policy, we generated 50 randomly generated environments, each starting from the same initial position at $(0, 0)$ m and featuring a randomly assigned goal position. Obstacles were placed within a 10×10 m area and varied in size, location, and shape (randomly selected from circles, ellipses, or polygons). Among these 50 scenarios, 10 contained no obstacles, while the remaining 40 were evenly distributed across those containing 1, 2, 6, or 8 obstacles (10 scenarios each). Fig. 3 illustrates five representative settings of these scenarios. Table I presents the hyper-parameters

used in the reinforcement learning process, and Table II shows scaling factors used in the reward design. The learning is performed on an Ubuntu 20.04 laptop with an NVIDIA RTX 4060 GPU.

TABLE I. RL hyper-parameters used in learning

Symbol	meaning	Value
γ	Discount factor	0.99
α_a	Learning rate (actor network)	$5e - 4$
α_c	Learning rate (critic network)	$1e - 3$
N	Batch size	64
D	Replay buffer size	100,000
η	target entropy	-0.5

TABLE II. Reward parameter value

Reward Parameters	Value
$[a_g, b_g]$	[2.33, 0.3]
a_θ	1.39
q_a	0.5
$[q_v, a_v, b_v]$	[0.7, 15, 0.5]
ζ	0.4

Data Bootstrapping. While the SAC algorithm promotes exploration through its off-policy formulation, its convergence to higher rewards can be hindered if initial explorations are ineffective (e.g., rarely reaching the goal). To address this, we initialize the replay buffer with a demonstration dataset to bootstrap online policy learning. Specifically, we leverage the linear LIP-MPC controller from our previous work [20], augmented with a Rapidly-exploring Random Tree (RRT) for enhanced global exploration (denoted as RRT-LMPC). The structure of RRT-LMPC is similar to our proposed hierarchical framework, in which RRT is responsible for generating subgoals for the LMPC. Specifically, we collected 10,000 state-action transactions from the RRT+LMPC controller across various training environments. During the early phase of training, 80% of the replay buffer samples are drawn from this offline demonstration dataset, while the remaining 20% originate from online interactions with the simulation environment. As training progresses, the reliance on the demonstration dataset is gradually reduced until the replay buffer is composed entirely (100%) of online samples. The overall training process spans 10,000 episodes. Results in the following section demonstrate that the data bootstrapping method significantly improves both learning convergence and navigation performance (e.g., success rate and travel time).

IV. SIMULATION RESULTS

This section details the simulation setup and presents the results that demonstrate the effectiveness and performance of the proposed method in navigating cluttered environments ¹.

Simulation Setup. We evaluate the performance and generalization of our approach in two testing environments: a

¹A video showing all simulation results can be found in the <https://youtu.be/cbz4vPvsF4g>.

testing-seen environment and a *testing-unseen* environment. The *testing-seen* environment comprises all navigation scenarios used during training, while the *testing-unseen* environment is designed to assess the generalization capability of the proposed method. Specifically, the *testing-unseen* environment consists of 25 newly generated scenarios created using the same randomization procedure as the training set; however, each unseen scenario contains eight obstacles (i.e., the maximum difficulty level) of varying shapes and sizes. In all *testing-unseen* cases, the robot starts at (0, 0) m and aims to reach the universal goal at (10, 10) m, which can increase the likelihood of encountering randomly generated obstacles, providing a more rigorous evaluation.

A. Comparisons against Baseline Model-Based Approaches

In this section, we evaluate the navigation performance of the proposed RL approach against three baseline model-based methods: a model-based nonlinear LIP-MPC controller [10], a linear LIP-MPC controller (denoted as LMPC) [20], and the RRT-LMPC—the expert approach used for collecting the demonstration dataset.

Real-Time Computation. The nonlinear LIP-MPC optimizes both stepping positions and turning rates based on the global goal position and obstacle information. However, the inherent nonlinearity of its optimization constraints results in an average computation time of 110 ± 57 ms per optimization, which is insufficient to achieve the necessary real-time update frequency—at least 20 Hz—for stable walking [33]. In contrast, the linear LIP-MPC (LMPC) efficiently computes gait controls in only 0.94 ± 0.07 ms, enabling real-time reactive gait generation. Despite this, LMPC may suffer from steering inflexibility due to its precomputation of turning rates [20]. To address this limitation, our high-level RL planner—and, alternatively, a global RRT planner—provides dynamic subgoals that guide the low-level LMPC. Notably, the RL planner computes a subgoal from the state and environmental feedback in just 1.3 ± 0.5 ms, which is adequate for our chosen frequency of 2.5 Hz (i.e., updating at every walking step). We intentionally maintain this lower update frequency, despite the fast computation times, to allow sufficient processing time for environmental and state feedback.

Navigation Performance. We evaluated the navigation performance of three methods—LMPC without subgoals, RRT+LMPC, and the proposed Subgoal Pursuit planner—across four trials in the *testing-seen* environments. Performance metrics included success rate, accumulated reward, and the average ratio of goal-reaching time (only considering successful trails) relative to our Subgoal Pursuit method. The comparison results are summarized in Table III, with results from one specific trail illustrated in Fig. 4.

From Table III, we observe that the linear MPC approach, being the most conservative, achieves the lowest success rate. Its limited ability to perform agile maneuvers often requires the robot to slow down or rely on side-walking to avoid obstacles, which increases the likelihood of time-outs or becoming trapped in local minima. The introduction

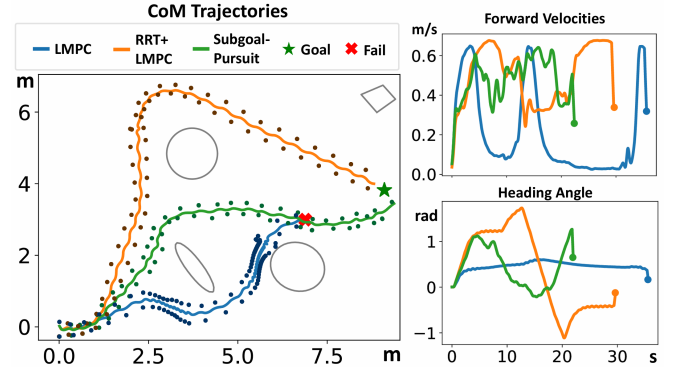


Fig. 4. The navigation performance of LMPC, RRT-LMPC, and Subgoal Pursuit planner in one specific environment. The right figure shows the resulted paths with stepping positions, and the left plots show the forward walking velocity and commanded turning rates.

TABLE III. The results of four trials in the *testing-seen* environment for each methods.

Method	Success rate [%]	Accumulated Reward	Time Ratio
LMPC	84 ± 0.0	91.06 ± 0.0	1.17
RRT+LMPC	90 ± 1.4	96.11 ± 3.64	1.02
Our method	93.3 ± 2.1	101.07 ± 2.41	1

of a global planner (e.g., RRT) improves the flexibility and success rate, as evidenced by higher cumulative rewards and average speed. However, the inherent randomness of RRT and its lack of consideration for the bipedal robot’s dynamic model often lead to the generation of overly aggressive subgoals, thereby limiting further improvements in success rate. In contrast, our proposed Subgoal Pursuit method achieves the highest success rate and accumulated reward among the three approaches, and it also reaches the goal fastest on average compared to the other two methods. Fig. 4 shows the navigation trajectories of the three approaches in a specific trail. In this case, LMPC fails due to a timeout caused by slow lateral walking. RRT+LMPC reaches the goal but follows the longest trajectory. Although RRT+LMPC maintains the highest forward velocity when moving straight, its efficiency is compromised by unnecessary detours. In contrast, the Subgoal Pursuit method achieves the goal the fastest by more smoothly regulating both the walking speed and turning rate.

By leveraging RL as a high-level planner, our algorithm determines robust subgoals through continuous exploration in the environment. Notably, bootstrapping the RL training with a model-based dataset results in final performance surpassing that of the original model-based approach, underscoring the strength of RL in navigation tasks. It is important to note that our approach relies solely on local map data, in contrast to the global map used by RRT. This reliance on local information introduces a slightly higher variance, which may also stem from the inherent randomness and uncertainty of the policy structure.

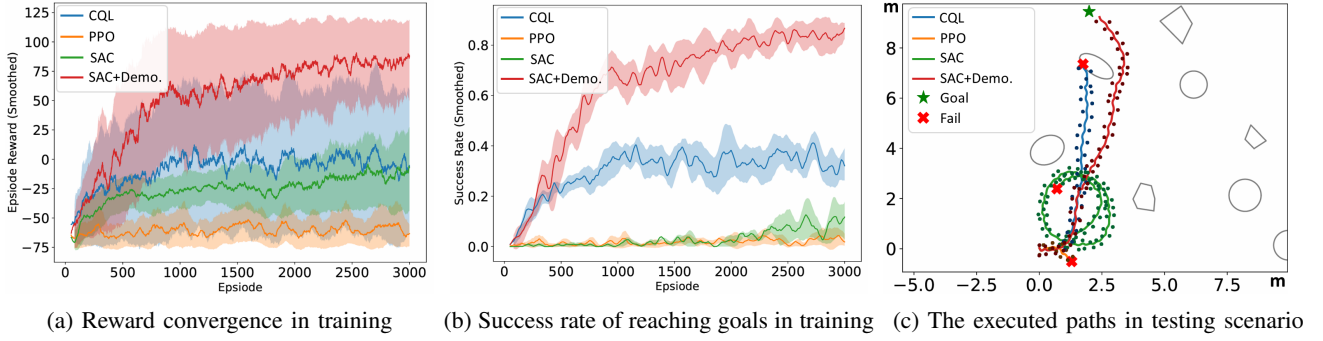


Fig. 5. Comparing training performance of four different learning-based approaches.

B. Comparison against Other Learning Based Methods

To identify the most effective RL algorithm for the high-level planning component of our Subgoal Pursuit framework, we evaluated several state-of-the-art learning-based methods. Each method was trained and tested under consistent conditions and compared based on key performance metrics such as success rate, accumulated reward, and average reaching time. The following sections provide detailed descriptions of these baseline algorithms and discuss their relative performance within our framework.

Conservative Q-Learning(CQL): CQL [34] is an offline RL algorithm that learns from pre-collected data by conservatively estimating Q-values, which helps ensure stability and reliability without the need for online interaction.

Proximal Policy Optimization (PPO): PPO [35] is an on-policy algorithm that uses a clipped objective function to constrain policy updates, ensuring stable training dynamics.

Soft Actor-Critic (SAC): SAC is an off-policy actor-critic algorithm that optimizes a stochastic policy with an entropy-augmented reward. In our tests, we use SAC as a baseline to showcase the benefits of bootstrapping online RL with prior demonstration data.

Fig. 5 shows the comparison of training outcomes of the four learning-based approaches: CQL, PPO, SAC, and SAC with demonstration. PPO consistently underperforms due to its on-policy nature limits sample efficiency in complex tasks. SAC benefits from its off-policy formulation, allowing it to reuse transitions more effectively. However, SAC’s training performance is highly sensitive to the quality of collected transitions. In our experiments, when the agent rarely reached the goal during exploration, SAC tended to wander in circles until timing out, as illustrated in Fig. 5c. Conversely, when the goal was reached more frequently, high-quality transitions stored in the replay buffer helped guide SAC toward a better policy. Consequently, SAC’s episodic reward often converged to levels comparable to CQL, while its average success rate remained relatively low.

CQL, benefiting from its offline RL formulation and efficient use of demonstration data, achieved faster improvements in both episodic reward and success rate during the early training stages. However, due to its lack of interaction with the environment during training, CQL struggled to adapt to dynamic environmental changes, leading to occa-

sional obstacle collisions, as shown in Fig. 5c. SAC with demonstration outperformed all other baselines by combining demonstration bootstrapping and interactive exploration. Leveraging offline demonstrations directed the agent toward more promising strategies early in training, thereby reducing the reliance on random exploration and avoiding suboptimal behaviors. This complementary effect accelerated learning and stabilized the training process, ultimately resulting in improved performance.

To further evaluate the performance and generalization of each learning-based approach, we tested the trained policies both in *testing-seen* environments and *testing-unseen* environments. The results are summarized in Table IV and Table V. We observe that SAC with demonstration achieves the highest success rate and accumulated reward in both testing, demonstrating superior performance and generalization over other baselines. PPO has difficulty learning navigation strategies in both cases due to its low sample efficiency. SAC has a slightly better performance than PPO in these tasks but is still significantly worse than SAC with demonstration. While CQL has lower success rates and accumulated rewards than our proposed approach in both testing, it results in the fastest time to reach the goal when successful.

TABLE IV. The results of four trials in the *testing-seen* environment for each method.

Method	Success rate [%]	Accumulated Reward	Time Ratio
CQL	44.3 ± 4.2	14.32 ± 5.97	0.91
PPO	0 ± 0	-73.43 ± 4.64	—
SAC	9 ± 2.6	-32.72 ± 3.57	1.01
SAC+Demo.	93.3 ± 2.1	101.07 ± 2.41	1

TABLE V. The results of four trials in the *testing-unseen* environment for each method.

Method	Success rate [%]	Accumulated Reward	Time Ratio
CQL	14 ± 8.2	-48 ± 3.53	0.92
PPO	0 ± 0	-75.43 ± 1.04	—
SAC	5 ± 2	-49.21 ± 2.09	1.08
SAC+Demo.	89.3 ± 2.2	101.47 ± 4.38	1

V. CONCLUSION

In this paper, we introduced the Subgoal-Pursuit method—a hierarchical navigation framework for bipedal robots that uses RL to learn a high-level planner to manage navigation complexity and used a model-based gait planner to ensure stable locomotion. In addition, we accelerated the training of the SAC algorithm by using a dataset bootstrapping technique. The results demonstrate its effectiveness in guiding bipedal robots through complex environments. However, there remains room for improving trajectory optimization and enhancing robustness and generalization to unseen and dynamic environments. Future work will focus on enhancing the learning framework to guarantee safe navigation in unseen and dynamic environments, as well as implementing the proposed approach on hardware for real-world validation.

REFERENCES

- [1] D. L. Wight, E. G. Kubica, and D. W. L. Wang, "Introduction of the Foot Placement Estimator: A Dynamic Measure of Balance for Bipedal Robotics," *Journal of Computational and Nonlinear Dynamics*, vol. 3, no. 1, p. 011009, 11 2007.
- [2] M. Wermelinger, P. Fankhauser, R. Diethelm, P. Krüsi, R. Siegwart, and M. Hutter, "Navigation planning for legged robots in challenging terrain," in *2016 IEEE/RSJ International Conference on Intelligent Robots and Systems (IROS)*. IEEE, 2016, pp. 1184–1189.
- [3] S. Kuindersma, R. Deits, M. Fallon, A. Valenzuela, H. Dai, F. Permenter, T. Koolen, P. Marion, and R. Tedrake, "Optimization-based locomotion planning, estimation, and control design for the atlas humanoid robot," *Autonomous robots*, vol. 40, pp. 429–455, 2016.
- [4] N. Sleumer and N. Tschichold-Gürmann, "Exact cell decomposition of arrangements used for path planning in robotics," *Technical Report/ETH Zurich, Department of Computer Science*, vol. 329, 1999.
- [5] N. Sariff and N. Buniyamin, "An overview of autonomous mobile robot path planning algorithms," in *2006 4th student conference on research and development*. IEEE, 2006, pp. 183–188.
- [6] A. Gasparetto, P. Boscariol, A. Lanzutti, and R. Vidoni, "Path planning and trajectory planning algorithms: A general overview," *Motion and Operation Planning of Robotic Systems: Background and Practical Approaches*, pp. 3–27, 2015.
- [7] Y. N. Kim, D. W. Ko, and I. H. Suh, "Confidence random tree-based algorithm for mobile robot path planning considering the path length and safety," *International Journal of Advanced Robotic Systems*, vol. 16, no. 2, p. 1729881419838179, 2019.
- [8] A. W. Winkler, "Optimization-based motion planning for legged robots," Ph.D. dissertation, ETH Zurich, 2018.
- [9] A. Shamsah, Z. Gu, J. Warnke, S. Hutchinson, and Y. Zhao, "Integrated task and motion planning for safe legged navigation in partially observable environments," *IEEE Transactions on Robotics*, vol. 39, no. 6, pp. 4913–4934, 2023.
- [10] C. Peng, V. Paredes, and A. Hereid, "Unified path and gait planning for safe bipedal robot navigation," *arXiv preprint arXiv:2403.17347*, 2024.
- [11] M. Diehl, H. G. Bock, H. Diedam, and P.-B. Wieber, "Fast direct multiple shooting algorithms for optimal robot control," in *Fast motions in biomechanics and robotics: optimization and feedback control*. Springer, 2006, pp. 65–93.
- [12] K. Mombaur, "Using optimization to create self-stable human-like running," *Robotica*, vol. 27, no. 3, pp. 321–330, 2009.
- [13] H. Dai, A. Valenzuela, and R. Tedrake, "Whole-body motion planning with centroidal dynamics and full kinematics," in *2014 IEEE-RAS International Conference on Humanoid Robots*. IEEE, 2014, pp. 295–302.
- [14] S. Kajita, F. Kanehiro, K. Kaneko, K. Yokoi, and H. Hirukawa, "The 3d linear inverted pendulum mode: A simple modeling for a biped walking pattern generation," in *Proceedings 2001 IEEE/RSJ International Conference on Intelligent Robots and Systems. Expanding the Societal Role of Robotics in the the Next Millennium (Cat. No. 01CH37180)*, vol. 1. IEEE, 2001, pp. 239–246.
- [15] J. Engelsberger, C. Ott, M. A. Roa, A. Albu-Schäffer, and G. Hirzinger, "Bipedal walking control based on capture point dynamics," in *2011 IEEE/RSJ international conference on intelligent robots and systems*. IEEE, 2011, pp. 4420–4427.
- [16] M. Rutschmann, B. Satzinger, M. Byl, and K. Byl, "Nonlinear model predictive control for rough-terrain robot hopping," in *2012 IEEE/RSJ International Conference on Intelligent Robots and Systems*. IEEE, 2012, pp. 1859–1864.
- [17] R. Grandia, F. Jenelten, S. Yang, F. Farshidian, and M. Hutter, "Perceptive locomotion through nonlinear model-predictive control," *IEEE Transactions on Robotics*, vol. 39, no. 5, pp. 3402–3421, 2023.
- [18] R. J. Griffin and A. Leonessa, "Model predictive control for dynamic footstep adjustment using the divergent component of motion," in *2016 IEEE International Conference on Robotics and Automation (ICRA)*. IEEE, 2016, pp. 1763–1768.
- [19] K. S. Narkhede, A. M. Kulkarni, D. A. Thanki, and I. Poulakakis, "A sequential mpc approach to reactive planning for bipedal robots using safe corridors in highly cluttered environments," *IEEE Robotics and Automation Letters*, vol. 7, no. 4, pp. 11 831–11 838, 2022.
- [20] C. Peng, V. Paredes, G. A. Castillo, and A. Hereid, "Real-time safe bipedal robot navigation using linear discrete control barrier functions," in *To appear in 2025 IEEE International Conference on Robotics and Automation (ICRA)*, 2025.
- [21] P. Abbeel and A. Y. Ng, "Apprenticeship learning via inverse reinforcement learning," in *Proceedings of the twenty-first international conference on Machine learning*, 2004, p. 1.
- [22] U. Syed, M. Bowling, and R. E. Schapire, "Apprenticeship learning using linear programming," in *Proceedings of the 25th international conference on Machine learning*, 2008, pp. 1032–1039.
- [23] J. Ho and S. Ermon, "Generative adversarial imitation learning," *Advances in neural information processing systems*, vol. 29, 2016.
- [24] R. Cimurs, J. H. Lee, and I. H. Suh, "Goal-oriented obstacle avoidance with deep reinforcement learning in continuous action space," *Electronics*, vol. 9, no. 3, p. 411, 2020.
- [25] B. Brito, M. Everett, J. P. How, and J. Alonso-Mora, "Where to go next: Learning a subgoal recommendation policy for navigation in dynamic environments," *IEEE Robotics and Automation Letters*, vol. 6, no. 3, pp. 4616–4623, 2021.
- [26] C. Pérez-D'Arpino, C. Liu, P. Goebel, R. Martín-Martín, and S. Savarese, "Robot navigation in constrained pedestrian environments using reinforcement learning," in *2021 IEEE International Conference on Robotics and Automation (ICRA)*. IEEE, 2021, pp. 1140–1146.
- [27] W. Zhu and M. Hayashibe, "A hierarchical deep reinforcement learning framework with high efficiency and generalization for fast and safe navigation," *IEEE Transactions on industrial Electronics*, vol. 70, no. 5, pp. 4962–4971, 2022.
- [28] Z. Xie and P. Dames, "Drl-vo: Learning to navigate through crowded dynamic scenes using velocity obstacles," *IEEE Transactions on Robotics*, vol. 39, no. 4, pp. 2700–2719, 2023.
- [29] Z. Huang, J. Wu, and C. Lv, "Efficient deep reinforcement learning with imitative expert priors for autonomous driving," *IEEE Transactions on Neural Networks and Learning Systems*, vol. 34, no. 10, pp. 7391–7403, 2022.
- [30] H. Yuan, Z. Mu, F. Xie, and Z. Lu, "Pre-training goal-based models for sample-efficient reinforcement learning," in *The Twelfth International Conference on Learning Representations*, 2024.
- [31] T. Hester, M. Vecerik, O. Pietquin, M. Lanctot, T. Schaul, B. Piot, D. Horgan, J. Quan, A. Sendonaris, I. Osband, *et al.*, "Deep q-learning from demonstrations," in *Proceedings of the AAAI conference on artificial intelligence*, vol. 32, no. 1, 2018.
- [32] T. Haarnoja, A. Zhou, P. Abbeel, and S. Levine, "Soft actor-critic: Off-policy maximum entropy deep reinforcement learning with a stochastic actor," in *International conference on machine learning*. Pmlr, 2018, pp. 1861–1870.
- [33] G. A. Castillo, B. Weng, S. Yang, W. Zhang, and A. Hereid, "Template model inspired task space learning for robust bipedal locomotion," in *2023 IEEE/RSJ International Conference on Intelligent Robots and Systems (IROS)*. IEEE, 2023, pp. 8582–8589.
- [34] A. Kumar, A. Zhou, G. Tucker, and S. Levine, "Conservative q-learning for offline reinforcement learning," *Advances in neural information processing systems*, vol. 33, pp. 1179–1191, 2020.
- [35] J. Schulman, F. Wolski, P. Dhariwal, A. Radford, and O. Klimov, "Proximal policy optimization algorithms," *arXiv preprint arXiv:1707.06347*, 2017.